Acta Pharmaceutica Sinica B 2023;13(2):678–693

Chinese Pharmaceutical Association
Institute of Materia Medica, Chinese Academy of Medical Sciences

Acta Pharmaceutica Sinica B

www.elsevier.com/locate/apsb
www.sciencedirect.com

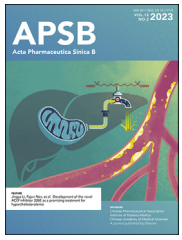

ORIGINAL ARTICLE

# Costunolide covalently targets NACHT domain of NLRP3 to inhibit inflammasome activation and alleviate NLRP3-driven inflammatory diseases

**Haowen Xu[a,b], Jiahao Chen[a], Pan Chen[a], Weifeng Li[a], Jingjing Shao[a,b], Shanshan Hong[a], Yi Wang[a], Lingfeng Chen[b], Wu Luo[a,c,*], Guang Liang[a,b,*]**

[a]*Chemical Biology Research Center, School of Pharmaceutical Sciences, Wenzhou Medical University, Wenzhou 325035, China*
[b]*School of Pharmaceutical Sciences, Hangzhou Medical College, Hangzhou 311399, China*
[c]*Medical Research Center, the First Affiliated Hospital of Wenzhou Medical University, Wenzhou 325000, China*

Received 10 May 2022; received in revised form 25 August 2022; accepted 23 September 2022

**KEY WORDS**

Costunolide;
NLRP3 inflammasome;
Inflammation;
Molecular target;
NACHT domain;
α-Methylene-γ-butyrolactone;
Gouty arthritis;
Ulcerative colitis

**Abstract** The NLRP3 inflammasome's core and most specific protein, NLRP3, has a variety of functions in inflammation-driven diseases. Costunolide (COS) is the major active ingredient of the traditional Chinese medicinal herb *Saussurea lappa* and has anti-inflammatory activity, but the principal mechanism and molecular target of COS remain unclear. Here, we show that COS covalently binds to cysteine 598 in NACHT domain of NLRP3, altering the ATPase activity and assembly of NLRP3 inflammasome. We declare COS's great anti-inflammasome efficacy in macrophages and disease models of gouty arthritis and ulcerative colitis *via* inhibiting NLRP3 inflammasome activation. We also reveal that the α-methylene-γ-butyrolactone motif in sesquiterpene lactone is the certain active group in inhibiting NLRP3 activation. Taken together, NLRP3 is identified as a direct target of COS for its anti-inflammasome activity. COS, especially the α-methylene-γ-butyrolactone motif in COS structure, might be used to design and produce novel NLRP3 inhibitors as a lead compound.

*Corresponding authors. Tel./fax: +86 577 86699396.
E-mail addresses: wzmcliangguang@163.com (Guang Liang), wuluo@wmu.edu.cn (Wu Luo).

Peer review under responsibility of Chinese Pharmaceutical Association and Institute of Materia Medica, Chinese Academy of Medical Sciences.

https://doi.org/10.1016/j.apsb.2022.09.014

## 1. Introduction

The nucleotide-oligomerization domain-like receptor (NLR) family pyrin domain-containing 3 (NLRP3) inflammasome, consisting of an innate immune sensor NLRP3, adaptor protein apoptosis-associated speck-like protein containing a CARD (ASC), and effector protein caspase-1, belongs to NLR family[1,2]. Assembly of NLRP3 inflammasome results in the cleavage of caspase-1 (p20), which promotes the cleavage of pro-interleukin (IL)-1$\beta$ and pro-IL-18 to generate mature and functional IL-1$\beta$ and IL-18[3], respectively. Cleaved caspase 1 also cleaves gasdermin D (GSDMD), which forms the lytic pore as the pyroptotic effector[4]. NLRP3 inflammasome can be activated by the stimulation of pathogen-associated molecular patterns (PAMPs) and death-associated molecular patterns (DAMPs)[5], which can further induce NLRP3 inflammasome activation *via* intracellular ionic fluxes[6,7], mitochondrial reactive oxygen species generation[8], or lysosomal damage[9]. NLRP3 consists of three domains, LRR, NACHT, and PYD domain. Generally, the assembly of NLRP3 is triggered in NLRP3 NACHT domain self-oligomerization induced by DAMPs and PAMPs. Next, the PYD domain of NLRP3 interacts with the PYD of adaptor protein ASC, which then leads to the formation of ASC speck. ASC speck recruits pro-caspase-1 *via* their homotypic CARD domains, eventually leading to the autocleavage and maturation of pro-caspase-1. The activation of caspase-1 causes the cleavage of IL-1$\beta$ and IL-18[10]. In addition, never in mitosis A-related kinase-7 (NEK7) has recently been characterized as a key component of NLRP3 inflammasome, which directly binds to and activates NLRP3 inflammasome[11]. Aberrant activation of NLRP3 inflammasome by DAMPs and PAMPs is associated with the progression of various inflammation-related diseases, such as colitis[12], gout arthritis[13], atherosclerosis[14], diabetic cardiomyopathy[15], and type 2 diabetes[16]. Pharmacological inhibition of NLRP3 can significantly alleviate inflammatory diseases[17]. However, only few small-molecule inhibitors of NLRP3 inflammasome are currently available for clinical use. Therefore, identification of small molecules targeting NLRP3 will aid in the development of novel NLRP3 inhibitors for the treatment of inflammatory diseases.

Natural products play a crucial role in drug discovery by providing a large number of lead compounds for drug design[18]. Costunolide (COS), a well-known sesquiterpene lactone, is divided from *Saussurea lappa*, a traditional Chinese herb often used to treat gastrointestinal diseases[19]. Recently, COS has been shown to possess antioxidative, anti-inflammatory, antiallergic, bone remodeling, neuroprotective, anticancer, and antidiabetic properties[20,21]. The anti-inflammatory activity of COS has been reported to be mainly attributed to its inhibition of the nuclear factor (NF)-$\kappa$B signaling pathway[20]. However, whether COS inhibits NLRP3 inflammasome activation and alleviates the NLRP3-mediated inflammatory diseases remains unclear. More importantly, the precise molecular targets of COS remain unknown.

In this study, we identified COS as an effective and selective inhibitor of NLRP3 inflammasome in an in-house bank of 119 natural compounds. We demonstrated that COS covalently binds to cysteine 598 (C598) of NACHT domain of NLRP3, inhibiting the ATPase activation of NLRP3 and exerting high anti-inflammasome activity in NLRP3-driven diseases. We also discovered that the $\alpha$-methylene-$\gamma$-butyrolactone motif in sesquiterpene lactone is an active group for binding to NLRP3, which may contribute to the design and development of novel NLRP3 inhibitors.

## 2. Materials and methods

### 2.1. Reagents

Lipopolysaccharides (LPS, #L2880), adenosine triphosphate (ATP, #A3377), and aluminum potassium sulfate dodecahydrate (Alum, #237086) were purchased from Sigma (St. Louis, MO, USA). COS was bought from Abphyto Biotech Co., Ltd. (Chengdu, China). MitoSOX (#M36008) was obtained from Invitrogen (Carlsbad, CA, USA). MitoTracker (#C1049B) and protein A + G agarose (#P2012) were supplied by Beyotime (Shanghai, China). Anti-NLRP3 (#AG-20B-0014) and anti-mouse caspase-1 (#AG-20B-0042) antibodies were purchased from Adipogen (San Diego, CA, USA). Anti-NEK7 (#ab133514) and anti-GSDMD (#ab209845) antibodies were obtained from Abcam (Cambridge, UK). Anti-mouse IL-1$\beta$ (#AF-401-NA) antibody was from R&D Systems (Minneapolis, MN, USA). Anti-Flag (#20543-1-AP), anti-HA (#66006-2-Ig), and anti-$\beta$-actin (#66009-1-Ig) antibodies were purchased from Proteintech (Rosemont, IL, USA).

### 2.2. Cell culture

Bone marrow-derived macrophages (BMDMs) were isolated and cultured as described[22]. In brief, an 8-week-old mouse was sacrificed and the femoral and tibial bones were cut off. The bone marrow cells were flushed out and cultured for 7 days in Dulbecco's modified Eagle's medium (DMEM, #C11995500BT; Gibco, Waltham, MA, USA) supplemented with 10% fetal bovine serum (FBS, #10270-106; Gibco), 20% supernatants of L929 mouse fibroblasts, 100 U/mL penicillin, and 100 mg/mL streptomycin (#C100C5; NCM Biotech, Suzhou, China). On Day 3 and Day 5, fresh media was added. L929 mouse fibroblasts (#GNM28) and HEK-293T cells (#GNHu17) were purchased from the Shanghai Institute of Biochemistry and Cell Biology (Shanghai, China). HEK-293T cells were cultured in DMEM supplemented with 10% FBS and antibiotics. L929 cells were cultured in minimum essential medium-$\alpha$ (#SH30265.01; Hyclone, Logan, UT, USA) supplemented with 10% FBS and antibiotics. Human peripheral blood mononuclear cells (PBMCs) were isolated from healthy volunteers using Human Peripheral Blood Monocyte Isolation Solution Kit (#P8680; Solarbio, Beijing, China). PBMCs were cultured overnight before stimulation in the Roswell Park Memorial Institute 1640 medium (#C11875500BT; Gibco) supplemented with 10% FBS and antibiotics. The procedures involving human PBMC samples were approved by the First Affiliated Hospital of Wenzhou Medical University in China and

all samples were obtained with informed consent (the ethical approval No. 2018-201).

### 2.3. Animal experiments

C57BL/6J mice used in the studies were obtained from Gempharmatech Co., Ltd. (Nanjing, Jiangsu, China). C57BL/6-*Nlrp3*$^{KO}$ mice (strain No.: VSM40005) and the littermate control mice were purchased from Beijing Viewsolid Biotech Co., Ltd. (Beijing, China). Mice were housed on a strict 12 h/12 h light/dark cycle (lights on at 8:00 a.m. and off at 8:00 p.m.) at 23 ± 2 °C and fed a standard rodent diet in a specific pathogen-free environment. All animal experimental protocols were approved by the Wenzhou Medical University Animal Policy and Welfare Committee (approved No.: wydw-2021-147).

To model and evaluate dextran sulfate sodium (DSS)-induced colitis, ten-week-old male C57BL/6 (littermate control mice) and *Nlrp3*$^{KO}$ mice were treated with 2.5% DSS (#0216011080; MP Biomedicals, Santa Ana, CA, USA) dissolved in the drinking water for six days and were then provided with normal drinking water for four days. Mice in the normal group were provided regular water. COS (40 mg/kg) was intraperitoneally injected into mice every day for 10 days. Control mice were injected with vehicles containing 95% phosphate buffered saline (PBS, #P1020; Solarbio) and 5% dimethyl sulfoxide (DMSO, #D8371; Solarbio) at the same time points. Body weight was measured at the same time every day. The disease activity index (DAI) was scored on a scale of 0−4 as follows: 0, normal stool; 1, soft stools; 2, dark mucoid stool; 3, liquid stool with slight bleeding; and 4, gross bleeding. Mice were sacrificed on Day 10 to measure the colon length and the colonic tissue was harvested. Sections of paraffin-embedded colon tissues were stained with hematoxylin and eosin (H&E) staining. 5 mg of colon tissue was weighed and added 0.2 mL of Tissue Protein Extraction Reagent (#AR0101; Boster, Wuhan, China). After grinding, the level of IL-1$\beta$ and caspase-1 in the tissue homogenate were tested by using enzyme-linked immunosorbent assay (ELISA) and Western blotting, respectively.

To establish and assess monosodium urate (MSU, #U2875; Sigma)-induced acute gouty arthritis, 8−10-week-old male C57BL/6 (littermate control) mice and *Nlrp3*$^{KO}$ mice were injected intraperitoneally with COS (40 mg/kg) twice at an interval of 30 min before the subcutaneous injection of MSU into the footpad. Footpad size was measured with a Vernier caliper at the indicated time points. After 6 h, the mice were sacrificed and the footpad tissues were harvested. The tissues were cultured in 1 mL of Opti-MEM (#31985070; Gibco) for 1 h at 37 °C and the protein levels of murine IL-1$\beta$ and caspase-1 were measured using ELISA and caspase-1 activity assay kit (#C1101; Beyotime), respectively.

To model and evaluate Alum-induced peritonitis, 8−10-week-old male C57BL/6 mice and *Nlrp3*$^{KO}$ mice received daily gavage with COS (40 mg/kg) dissolved in 0.5% carboxymethylcellulose sodium three times before intraperitoneal injection of Alum (1 mg per mouse). After 12 h, the mice were sacrificed and 5 mL of PBS was used to wash the peritoneal cavities. The neutrophils in peritoneal were analyzed by flow cytometry by staining Per-CP-Ly6G antibody (#127653; BioLegend, San Diego, CA, USA) and FITC-CD45.2 antibody (#103108; BioLegend). The protein levels of murine IL-1$\beta$ and p20 in the peritoneal cells were measured using Western blotting.

To model and assess LPS-challenged mice, 8−10-week-old male C57BL/6 mice were intraperitoneally injected with COS (40 mg/kg) or vehicles containing 95% PBS and 5% DMSO. After 1 h, mice were intraperitoneally injected with LPS (10 mg/kg). After 4 h, serum samples were collected, and cytokines were measured using ELISA.

### 2.4. Inflammasome stimulation

To activate NLRP3 inflammasome, $1 \times 10^6$/mL of BMDMs or PBMCs were plated in 6-well plates. After overnight incubation, the BMDMs were primed with 500 ng/mL LPS for 3 h. Subsequently, the cells were treated with COS for 30 min, and then stimulated with ATP (2.5 mmol/L) and nigericin (10 μmol/L) for 30 min or Alum (300 μg/mL) for 4 h. PBMCs were treated with COS for 30 min and then stimulated with LPS for 16 h after overnight culture.

To stimulate the absence in melanoma 2 (AIM2) and NLR family CARD domain containing 4 (NLRC4) inflammasomes, after LPS priming and treatment with COS, BMDMs were transfected with poly (dA:dT) (#tlrl-patn; InvivoGen, Hong Kong, China) for 4 h using Lipofectamine 2000 (#11668500; Invitrogen) or stimulated with *Salmonella typhimurium* for 4 h.

### 2.5. Fluorescence staining

BMDMs were plated overnight in glass-bottom cell culture dishes at $1 \times 10^6$/mL density. In the following days. The next day, BMDMs were primed with 500 ng/mL of LPS for 3 h, treated with COS for 30 min, stimulated with 2.5 mmol/L ATP, and stained with MitoSOX (5 μmol/L) and MitoTracker (20 nmol/L) for 30 min. The cells were then washed thrice with PBS and fixed with 4% paraformaldehyde for 20 min at room temperature. After washing thrice with PBS containing 0.05% Tween-20 (PBST) and counterstaining with 4′,6-diamidino-2-phenylindole (DAPI, #36308ES11; Yeasen, Shanghai, China), the cells were observed under a fluorescence microscope (Nikon, Tokyo, Japan).

### 2.6. ELISA for cytokine examination

Supernatants from cell culture, footpad tissue culture, colon homogenate, and serum were detected for mouse IL-1$\beta$ (#88-7013-77), IL-6 (#88-7064-76), tumor necrosis factor (TNF)-$\alpha$ (#88-7324-76), and human IL-1$\beta$ (#88-7046-86) using commercial ELISA kits (Invitrogen) according to the manufacturer's instructions.

### 2.7. Intracellular chloride detection

BMDMs ($5 \times 10^5$/mL) were plated in a 12-wells plate and prepared following treatment and then stimulated with ATP at different times. After washing with PBS, the cells were lysed with ultrapure water for 15 min at 37 °C. After collection and centrifugation, 5 μmol/L N-(ethoxycarbonylmethyl)-6-methoxyquinolinium bromide (MQAE, #S1082; Beyotime) was added to the supernatants and the fluorescence intensity was measured using SpectraMax iD3 (Molecular Devices, San Jose, CA, USA).

### 2.8. Intracellular potassium detection

BMDMs ($1 \times 10^6$/mL) were plated in a 6-wells plate and prepared following treatment, and then stimulated with ATP. After washing thrice with 0.9% normal saline, the cells were lysed with ultrapure

water for 15 min at 37 °C. After collection and centrifugation, the supernatant was analyzed for potassium concentration using an AU5800 Clinical Chemistry Analyzer (Beckman Coulter, Indianapolis, IN, USA).

### 2.9. Western blotting and co-immunoprecipitation

Total protein from cells and tissues was extracted using lysis buffer (#AR0103; Boster). The cells culture supernatant was added to an equal volume of methanol and one-quarter volume of chloroform. After vortex and centrifugation, the upper solution was removed and the same volume of methanol was added. After vortex and centrifugation, the protein precipitation was resuspended in SDS sample loading buffer. The samples were separated using 12% sodium dodecyl sulfate (SDS)-polyacrylamide gel electrophoresis and then transferred to polyvinylidene fluoride membranes. Before adding specific primary antibodies, membranes were blocked in Tris-buffered saline (pH 7.4, containing 0.05% Tween 20 and 5% non-fat milk) for 1.5 h at room temperature. Protein bands were then detected by incubating with horseradish peroxidase-conjugated secondary antibodies and enhanced chemiluminescence reagent (Bio-Rad, Hercules, CA, USA). The density of the immunoreactive bands was analyzed using Image J software (NIH, Bethesda, MD, USA).

In co-immunoprecipitation assays, cell lysates prepared following treatments were incubated with decoy antibodies overnight at 4 °C, and immunoprecipitated with protein A + G agarose beads at 4 °C for 4 h. Immunoprecipitation samples were further subjected to immunoblotting for the detection of co-precipitated proteins. Total lysates were also performed for Western blot analysis as input control.

### 2.10. NLRP3 oligomerization assay

BMDMs prepared following treatments were lysed using lysis buffer (0.5% Triton X-100, 50 mmol/L Tris−HCl, 150 mmol/L NaCl, 10% glycerol, and protease inhibitor cocktail). After centrifugation, the precipitate was resuspended in 1 × sample buffer (0.5 × Tris-borate EDTA [TBE], 10% glycerol, 2% SDS containing 0.0025% bromophenol blue) and electrophoresed on a vertical 1.5% agarose gel in running buffer (1 × TBE and 0.1% SDS) for 1 h. The proteins were then transferred to polyvinylidene fluoride membranes for immunoblotting.

### 2.11. ASC oligomerization assay

BMDMs prepared following treatments were lysed using the lysis buffer (0.5% Triton X-100 and protease inhibitor cocktail in PBS). After centrifugation, the precipitate was resuspended in PBS, 2 mmol/L suberic acid bis (3-sulfo-*N*-hydroxysuccinimide ester) sodium salt (BS3, #S855494; Macklin, Shanghai, China) was added for crosslinking oligomer. After incubation at room temperature for 30 min and centrifugation, the pellets were resuspended in SDS sample loading buffer and analyzed using immunoblotting, as previously described.

### 2.12. Lactate dehydrogenase (LDH) assay

The release of LDH from BMDMs was detected by the LDH Cytotoxicity Assay Kit (#C0016; Beyotime) following the manufacturer's instructions.

### 2.13. Pull-down assay

Streptavidin-covered Beads (#22308-1; Beaver, Suzhou, China) were incubated with COS or biotinylated costunolide (bio-COS) for 30 min at room temperature. After washing with PBST, the beads were incubated with the cell lysates of LPS-primed BMDMs or plasmid-transfected HEK-293T cells for 6 h, washed with PBST, and the bound and total proteins were analyzed by Western blotting.

### 2.14. Cell-free surface plasmon resonance (SPR) and bio-layer interferometry (BLI) assay

For SPR, the binding affinity of COS for rhNLRP3-NACHT (#TP20536; Huabio, Hangzhou, China) was determined using a Biacore T200 instrument (GE, Boston, MA, USA) with a CM7 sensor chip. Briefly, recombinant proteins were loaded to the sensors using the Amine Coupling Kit (#BR100050; Cytiva, Boston, MA, USA). Concentration-gradient COS samples were prepared in a running buffer (PBS containing 0.05% P20, 5% DMSO). The sensor and sample plates were placed on the instrument, and COS samples flowed over the target sensors. Five concentrations were injected successively at a flow rate of 30 μL/min for a 200 s association phase, which was followed by an 80 s dissociation phase at 25 °C. The final graphs were obtained by subtracting blank sensor and blank samples in duplex. Data were analyzed using Biacore T200 software EV (GE).

For BLI, the binding affinity of COS for rhNLRP3-NACHT was determined using a ForteBio Octet Red system (ForteBio, San Francisco, CA, USA). The recombinant protein was biotinylated using the ReadiLink Protein Biotinylation Kit (#AAT-5520; AAT Bioquest, Sunnyvale, CA, USA) and immobilized onto Super Streptavidin Biosensors (#18-5057; ForteBio), and the association and dissociation of COS were monitored for 100 s, respectively. The final graphs were obtained by subtracting the blank sensor and blank samples in the duplex. Data were analyzed using ForteBio's Data Analysis Software version 8.1 software (ForteBio).

### 2.15. NLRP3 ATPase activity assay

Human NLRP3 immunoprecipitated from plasmid-transfected HEK-293T cells were incubated with different concentrations of COS for 40 min, then ultra-pure ATP was added to the reaction buffer and incubated at 37 °C for 40 min. The amount of ATP converted into ADP was determined by luminescent ATP detection with ADP-Glo Kinase Assay Kit (#V6930; Promega, Madison, WI, USA) according to the manufacturer's protocol.

### 2.16. Identification of modified peptides using mass spectrometry

Murine Flag-NLRP3 was transfected into HEK-293T cells using polyethyleneimine. After 24 h, cells were collected and resuspended in the lysis buffer. Extracts were immunoprecipitated with anti-Flag antibody and protein A + G beads and then dissolved in loading buffer. Proteins were separated using 12% SDS-PAGE and the gel was stained with Coomassie brilliant blue. Bands between 130 and 100 kDa were cut and digested with trypsin. Tryptic peptides were separated on a C18 column and were analyzed using an LTQ-Orbitrap-Velos mass spectrometer. Spectral data were then searched against the human protein RefSeq database in Proteome Discoverer with Mascot software.

### 2.17. Molecular docking

The molecular docking of NLRP3 NACHT domain oligomerization or COS to NACHT domain was performed using HADDOCK and AutoDock 4.2.6, respectively. The crystal structure of human NLRP3 NACHT domain (PDB ID: 7ALV) was obtained from Protein Data Bank (PDB). The AutoDock Tools version 1.5.6 package was applied to generate the docking input files and to analyze the docking results. We implemented a 60 × 60 × 60-point grid box with 0.375 Å spacing between the grid points. The affinity maps of NACHT were calculated by AutoGrid. One hundred Lamarckian genetic algorithm runs with default parameter settings were processed. Then the interactions of the protein and the ligand in the complex were analyzed by Independent Gradient Model[23,24].

### 2.18. Chemical synthesis of COS derivatives

For synthesis of reduced Costunolide (r-COS), COS (100 mg, 0.43 mmol) was dissolved in methanol. After adding 20 eq. sodium borohydride (325.68 mg), the mixture was stirred for 1 h at room temperature. After extraction by dichloromethane, the extract was purified by column chromatography, eluting with petroleum ether-ethyl acetate ($v/v$ = 2:1), to give the desired product r-COS (47.00 mg, 46.60%) as a white solid. HPLC purity of r-COS: 98.5%. Structural characterization of r-COS: $^1$H NMR (400 MHz, chloroform-$d$ ) $\delta$ 4.85 (dd, $J$ = 11.4, 4.4 Hz, 1H), 4.68 (d, $J$ = 10.0 Hz, 1H), 4.59 (dd, $J$ = 9.9, 8.5 Hz, 1H), 2.42 (dd, $J$ = 13.4, 6.3 Hz, 1H), 2.36−2.16 (m, 4H), 2.06 (tdd, $J$ = 13.1, 9.8, 2.9 Hz, 2H), 1.90 (ddd, $J$ = 13.9, 6.3, 2.1 Hz, 1H), 1.72 (s, 3H), 1.70−1.66 (m, 1H), 1.65−1.60 (m, 1H), 1.45 (s, 3H), 1.29 (d, $J$ = 6.9 Hz, 3H).

For synthesis of bio-COS, COS (50.00 mg, 0.22 mmol) was mixed with 1.5 eq. 1-ethyl-3-(3-dimethylaminopropyl) carbodiimide and 0.2 eq. 4-dimethylaminopyridine in acetonitrile, and D-biotin (73.79 mg, 0.30 mmol) was added into the mixture. The reaction was stirred at reflux temperature for 4 h. After extraction by dichloromethane, the extract was purified by column chromatography, eluting with dichloromethane-methanol ($v/v$ = 20:1) to give bio-COS (23.00 mg, 24.07%) as a white solid. HPLC purity of bio-COS: 97.9%. Structural characterization of bio-COS: $^1$H NMR (400 MHz, chloroform-$d$ ) $\delta$ 6.21 (d, $J$ = 3.4 Hz, 1H), 5.58 (t, $J$ = 8.3 Hz, 1H), 5.49 (d, $J$ = 3.1 Hz, 1H), 5.10 (d, $J$ = 10.2 Hz, 1H), 4.71−4.58 (m, 2H), 4.54 (t, $J$ = 6.3 Hz, 1H), 4.47 (d, $J$ = 12.3 Hz, 1H), 4.34 (dd, $J$ = 7.9, 4.5 Hz, 1H), 3.18 (q, $J$ = 6.6, 5.3 Hz, 1H), 3.01−2.90 (m, 1H), 2.77 (d, $J$ = 12.8 Hz, 1H), 2.63 (ddd, $J$ = 12.5, 9.1, 3.6 Hz, 1H), 2.36 (t, $J$ = 7.4 Hz, 2H), 2.33−1.99 (m, 7H), 1.97−1.90 (m, 1H), 1.89 (d, $J$ = 1.3 Hz, 3H), 1.80−1.63 (m, 5H), 1.58 (dt, $J$ = 14.5, 2.9 Hz, 1H), 1.47 (t, $J$ = 7.9 Hz, 2H).

### 2.19. Statistical analysis

Data are presented as the mean ± standard error of the mean (SEM). The statistical significance of differences between groups was determined using the Student's $t$-test or ANOVA multiple comparisons in GraphPad Prism 8 (GraphPad, San Diego, CA, USA). Differences are significant at $P < 0.05$.

## 3. Results

### 3.1. COS inhibits NLRP3 inflammasome activation

To uncover the anti-inflammatory compounds targeting pyroptosis, 119 natural compounds housed in our lab (Supporting Information Table S1) were screened for their inhibitory activity against NLRP3-driven IL-1$\beta$ production in LPS/ATP-challenged BMDMs (Fig. 1A). Interestingly, COS (Fig. 1B) showed the highest inhibitory rate (87.6%) on IL-1$\beta$ release among the 119 natural compounds. The cell viability assay showed that COS was not cytotoxic at concentrations below 10 μmol/L (Supporting Information Fig. S1A). Then we examined whether COS (at 1, 2, and 5 μmol/L) inhibited p20 cleavage and IL-1$\beta$ secretion in BMDMs to validate the inhibitory effects of COS on inflammasome activation. We found that COS suppressed p20 cleavage and IL-1$\beta$ release in a dose-dependent manner (Fig. 1C, D, and Fig. S1B). In addition, COS at 1, 2, and 5 μmol/L did not alter TNF-$\alpha$ and IL-6 levels in the culture supernatants of BMDMs (Fig. 1E and Fig. S1C). Actually, COS could decrease IL-1$\beta$ in LPS-primed BMDMs at lower doses ($IC_{50}$ = 0.66 μmol/L) than TNF-$\alpha$ ($IC_{50}$ > 10 μmol/L) (Supporting Information Fig. S2A and S2B). Furthermore, COS inhibited inflammasome-induced GSDMD activation and LDH release in BMDMs (Fig. 1F and G, and Supporting Information Fig. S3). Similar inhibition of IL-1$\beta$ production by COS was observed in human PBMCs (Fig. 1H). These data indicate that COS prevents NLRP3 inflammasome activation rather than regulating the production of NLRP3, pro-IL-1$\beta$, and inflammasome-independent inflammatory cytokines. These results were validated in mouse serum. The data in Supporting Information Fig. S4A and S4B show that COS administration significantly reduced serum IL-1$\beta$ production, but not TNF-$\alpha$ production, in LPS-challenged mice.

COS has been reported to have anti-inflammatory effects in LPS-challenged macrophages[25,26]. We then examined whether COS affected LPS-induced priming for NLRP3 inflammasome activation. When BMDMs were treated with COS at 1−5 μmol/L before LPS challenge, COS significantly suppressed LPS-induced pro-IL-1$\beta$ and NLRP3 expression, which is consistent with the previous report that COS could reduce LPS-induced pro-IL-1$\beta$ expression *via* inhibiting NF-$\kappa$B[25]. However, COS treatment after LPS challenge reduced p20 and pro-IL-1$\beta$ levels but failed to suppress LPS-induced pro-IL-1$\beta$ and NLRP3 expression, suggesting that COS could independently suppress NLRP3 activation without inhibiting LPS-induced priming signal (Fig. 1C, and Supporting Information Fig. S5A and S5B).

To explore the effects of COS on the activation of other inflammasomes, we also tested whether COS could inhibit IL-1$\beta$ secretion and p20 cleavage induced by the activators of other inflammasomes. As shown in Supporting Information Fig. S6A−S6D, COS failed to inhibit the activation of NLRC4 and AIM2 inflammasomes. Next, we explored whether COS could suppress NLRP3 inflammasome activation induced by other activators, such as nigericin and Alum[9]. We found that COS treatment also inhibited IL-1$\beta$ and p20 secretion triggered by nigericin and Alum in BMDMs (Fig. 1I and J, Supporting Information S7A and S7B). These findings indicate that COS may be a selective and effective inhibitor of NLRP3 inflammasome.

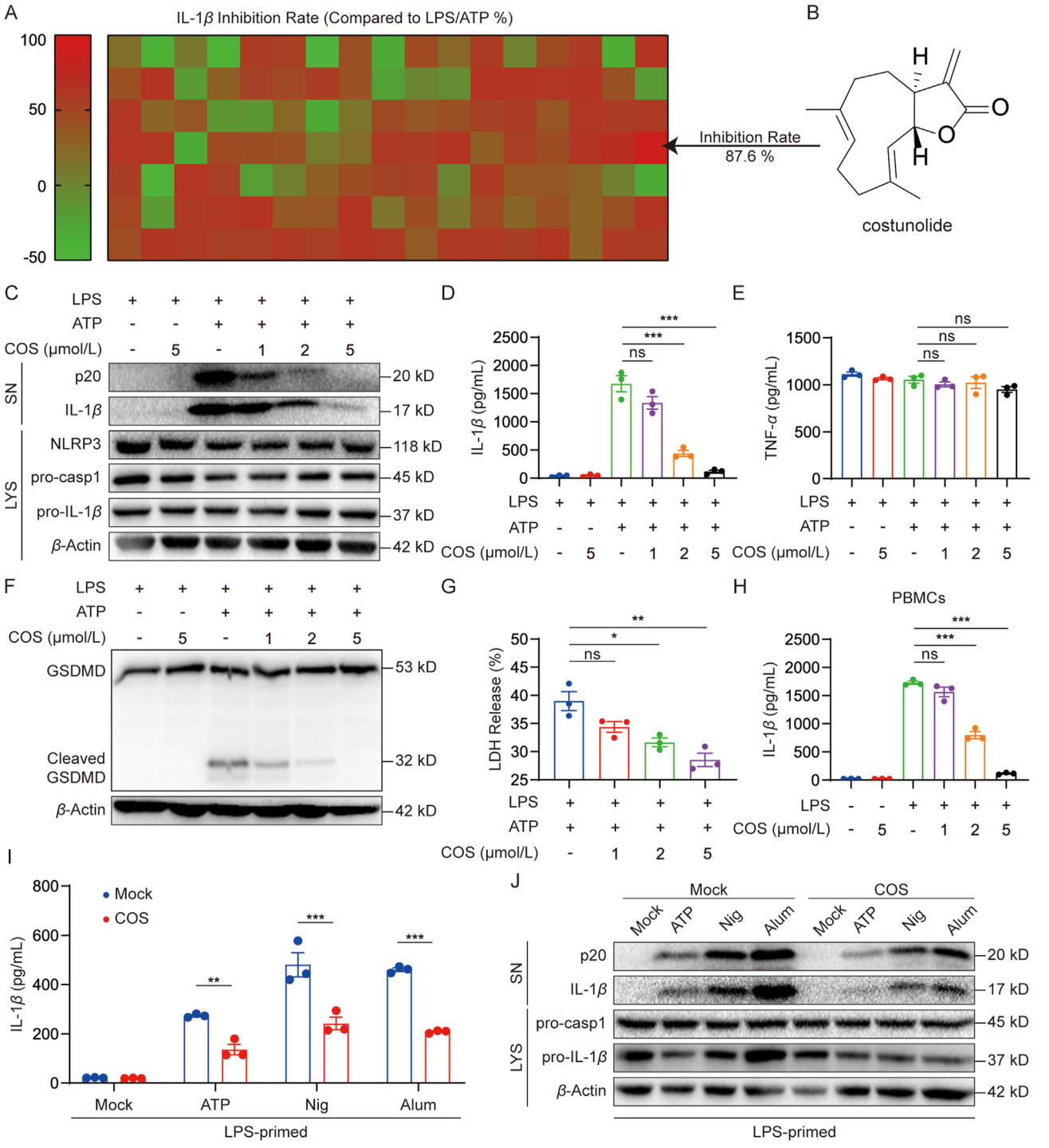


**Figure 1** COS inhibits NLRP3 inflammasome activation. (A) BMDMs were primed with LPS for 3 h and stimulated with ATP for 0.5 h after treatment with 5 μmol/L natural products library (119 compounds) for 0.5 h, ELISA of IL-1$\beta$ in culture supernatant (SN). (B) Structure of COS. (C–E) LPS-primed BMDMs were treated with or without COS in different doses for 0.5 h and then stimulated with ATP for 0.5 h. Western blotting analysis of cleaved IL-1$\beta$ and p20 levels in culture SN and pro-IL-1$\beta$, pro-caspase-1, and $\beta$-actin in lysates (Input) of BMDMs (C). IL-1$\beta$ (D) or TNF-$\alpha$ (E) production was assessed using ELISA in SN. (F) BMDMs were primed with LPS for 3 h and then stimulated with ATP for 0.5 h after treatment with various doses of COS (1, 2, and 5 μmol/L) for 0.5 h. Western blotting analysis of GSDMD, or cleaved-GSDMD in lysates. (G) Assay of LDH release in the culture supernatants of LPS-primed BMDMs treated with different doses of COS for 0.5 h and then stimulated with ATP for 1 h. (H) ELISA of IL-1$\beta$ in SN of PBMCs isolated from three healthy donors, treated with various doses of COS for 30 min, and then stimulated with LPS for 16 h. (I, J) LPS-primed BMDMs were treated with or without COS (2 μmol/L) for 0.5 h and then stimulated with ATP for 0.5 h, nigericin for 0.5 h, or Alum for 4 h. Western blotting analysis of mature IL-1$\beta$ and p20 levels in SN (I) or ELISA of IL-1$\beta$ production in SN (J). Data are presented as the mean ± SEM, $n = 3$; $^{*}P < 0.05$, $^{**}P < 0.01$, $^{***}P < 0.001$; ns, not significant.

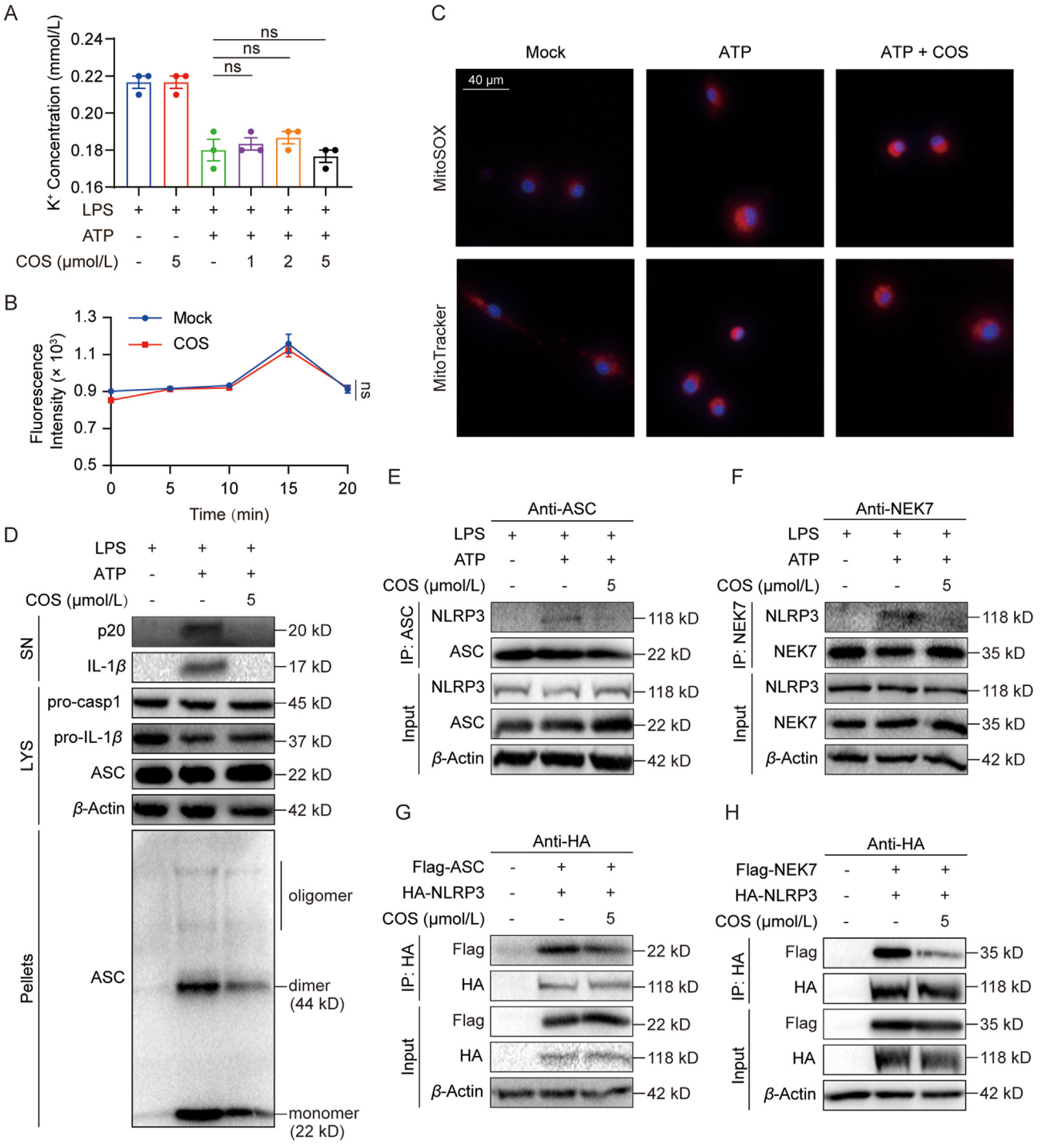


**Figure 2** COS inhibits NLRP3 inflammasome assembly. (A) Detection of potassium efflux in LPS-primed BMDMs treated with various doses of COS (1, 2, and 5 μmol/L) for 0.5 h and stimulated with ATP for 0.5 h. (B) Detection of chloride efflux in LPS-primed BMDMs treated with COS (5 μmol/L) for 0.5 h and stimulated with ATP at different time points. (C) Fluorescence analysis of LPS-primed BMDMs treated with COS for 0.5 h and stimulated with ATP for 0.5 h, followed by staining with MitoSOX, MitoTracker, and DAPI. (D) Western blotting analysis of ASC oligomerization in 0.5% Triton X-100 (pellets) of LPS-primed BMDMs treated with or without COS for 0.5 h and stimulated with ATP for 0.5 h. (E) Co-immunoprecipitation (Co-IP) with ASC antibody and western blotting analysis to evaluate the NLRP3−ASC interaction in LPS-primed BMDMs treated with or without COS for 0.5 h and stimulated with ATP for 0.5 h. (F) Co-IP with NEK7 antibody and Western blotting analysis to evaluate the NLRP3−NEK7 interaction in LPS-primed BMDMs treated with or without COS for 0.5 h and stimulated with ATP for 0.5 h. (G) Co-IP with HA antibody and Western blotting analysis to evaluate the NLRP3−ASC interaction in HEK-293T cells transfected with the high expression plasmid and treated with COS (5 μmol/L) for 16 h. (H) Co-IP with HA antibody and Western blotting analysis to evaluate the NLRP3−NEK7 interaction in HEK-293T cells transfected with the high expression plasmid and treated with COS (5 μmol/L) for 16 h. Data are presented as the mean ± SEM, $n = 3$; $^{**}P < 0.01$, $^{***}P < 0.001$; ns, not significant.

### 3.2. *COS inhibits NLRP3 inflammasome assembly*

Next, we attempted to understand how COS blocks NLRP3 activation. We then observed the effects of COS on upstream signaling events of NLRP3 inflammasome. The results showed that COS failed to affect ATP-induced potassium or chloride efflux (Fig. 2A and B) and mitochondrial damage (Fig. 2C). ASC oligomerization participates in the assembly of NLRP3 inflammasome, which is an important step of the subsequent caspase-1 activation[27]. We discovered that COS suppressed ATP-induced ASC oligomerization (Fig. 2D, Supporting Information Fig. S8A and S8B). These results indicate that COS inhibits NLRP3 inflammasome activation possibly by suppressing the assembly of inflammasome components.

We further validated the inhibition of COS on the endogenous interaction between NLRP3 and ASC in BMDMs (Fig. 2E). Recently, NEK7 has been defined as a license for NLRP3 activation *via* kinase-independent activation[11]. We observed that COS

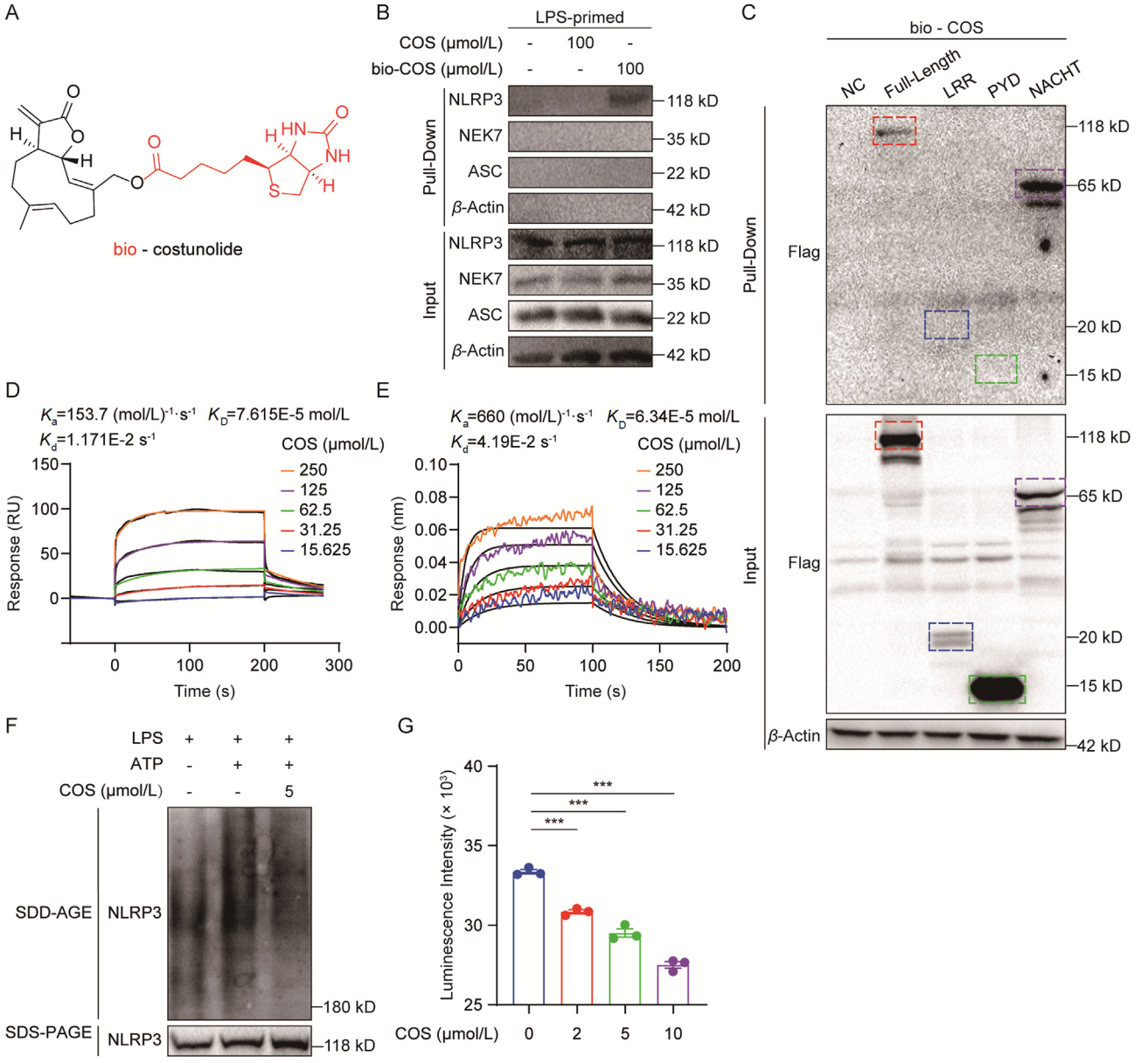


**Figure 3** COS directly targets NLRP3 NACHT domain. (A) Structure of biotinylated costunolide (bio-COS). (B) Streptavidin-covered beads with biotin and COS or bio-COS were incubated with the cell lysates of LPS-primed BMDMs for 6 h. As indicated, the levels of bound proteins (Pull-down) and total proteins (Input) were determined using Western blotting. (C) Streptavidin-covered beads with biotin and COS or bio-COS were incubated with the cell lysates of HEK-293T cells transfected with high expression plasmid of Flag-NLRP3-PYD, Flag-NLRP3-NACHT, and Flag-NLRP3-LRR for 6 h. As indicated, the levels of bound proteins (Pull-down) and total proteins (Input) were determined using Western blotting. (D) Binding affinity of COS with rhNLRP3-NACHT was determined using an SPR assay. (E) Binding affinity of COS with rhNLRP3-NACHT was determined using a BLI assay. (F) Western blotting analysis of NLRP3 by SDD-AGE or SDS-PAGE assay in LPS-primed BMDMs treated with COS for 0.5 h and stimulated with ATP for 0.5 h. (G) ATPase activity assay for endogenous NLRP3 proteins in the presence of different concentrations of COS. Data are presented as the mean ± SEM, $n = 3$; ***$P < 0.001$.

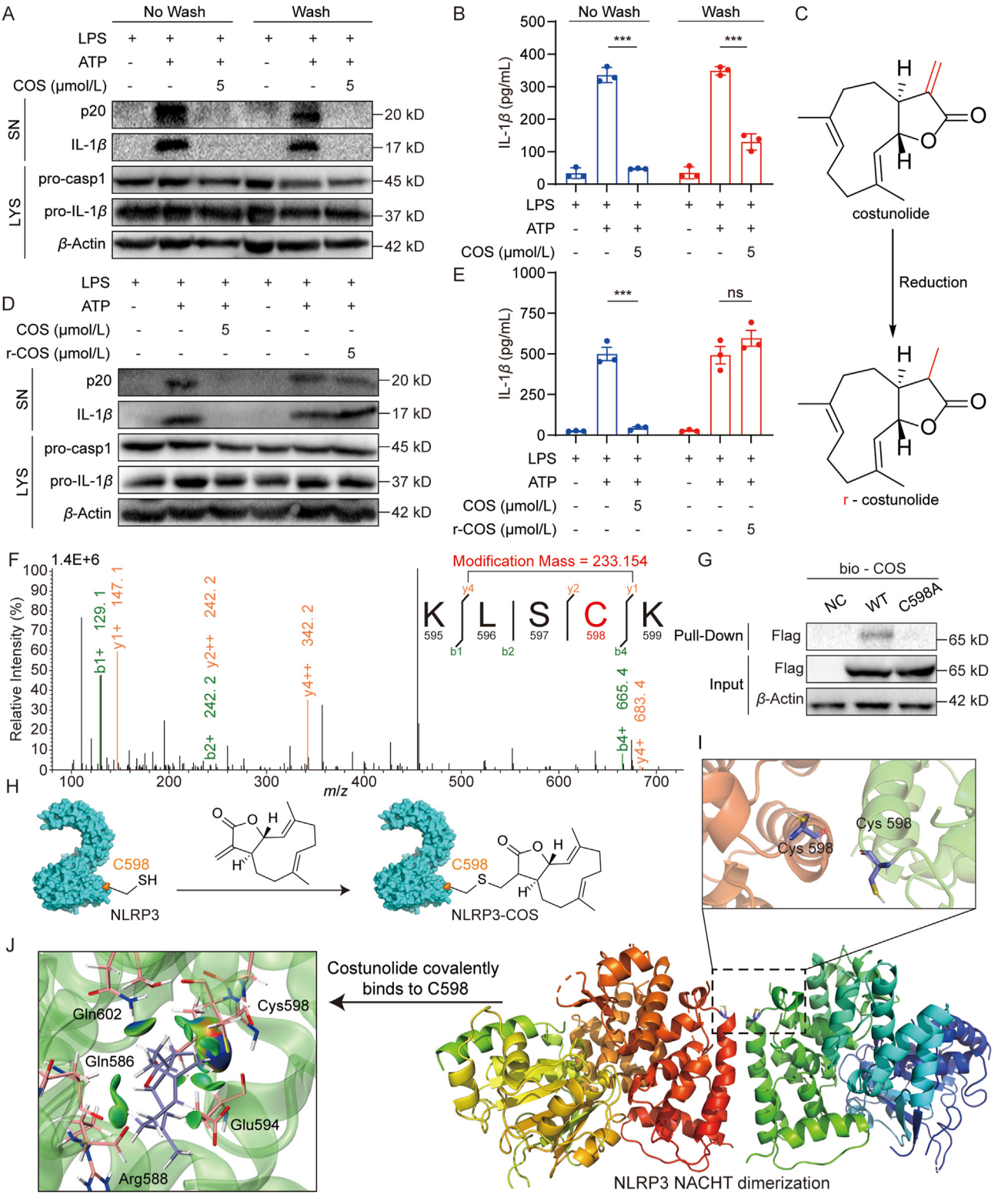


**Figure 4** COS covalently targets cysteine 598 on the NLRP3 NACHT domain. (A, B) LPS-primed BMDMs were treated with COS for 15 min and washed out, then stimulated with ATP for 0.5 h. Western blotting analysis of cleaved IL-1$\beta$ and p20 in SN (A) or ELISA of IL-1$\beta$ in SN (B). (C) The structure of reduced-costunolide (r-COS). (D, E) LPS-primed BMDMs were treated with or without COS or r-COS for 0.5 h, then stimulated with ATP for 0.5 h. Western blotting analysis of cleaved IL-1$\beta$, p20 in SN (D) or ELISA of IL-1$\beta$ in SN (E) from BMDMs. (F) Mass spectrogram of the modified peptide in endogenous NLRP3 treated with COS (5 μmol/L). (G) Streptavidin-covered beads with bio-COS were incubated with the cell lysates of HEK-293T cells transfected with the high expression plasmid of WT or cysteine 598 mutation to alanine (C598A) NACHT protein for 6 h. As indicated, the levels of bound proteins (Pull-down) and total proteins (Input) were determined using Western blotting. (H) Proposed model for the reaction between COS and cysteine 598 (C598) residue of NLRP3 (PDB ID: 6NPY). (I) Molecular docking

also suppressed the interaction of NLRP3 and NEK7 in BMDMs (Fig. 2F). After co-transfection of plasmids encoding NLRP3 and ASC or NLRP3 and NEK7 in HEK-293T cells, we confirmed that COS inhibited the interaction of these two complexes in NLRP3 inflammasome (Fig. 2G and H). Based on these results, we concluded that COS intervenes in the assembly of NLRP3 inflammasome and hypothesized that COS may directly target the core components of NLRP3 inflammasome.

### 3.3. *COS directly interacts with NLRP3 NACHT domain*

In order to identify the COS-targeting protein in NLRP3 inflammasome, bio-COS (Fig. 3A) was used for pull-down assay in cell lysates of BMDMs. As shown in Fig. 3B, NLRP3, rather than NEK7 and ASC, was pulled down by bio-COS, indicating that NLRP3 is a direct interacting target of COS. We validated the COS−NLRP3 interaction by pulling down HEK-293T cells transfected with Flag-labelled NLRP3 plasmid (Fig. 3C). In addition, the pull-down assay showed that the interaction between NLRP3 and bio-COS could be competitively reversed by free COS in a dose-dependent manner (Supporting Information Fig. S9).

Furthermore, we constructed plasmids encoding different domains to identify the COS-targeting domain of NLRP3. Interestingly, among these three domains, only NACHT domain of NLRP3 was pulled down by bio-COS, suggesting that COS targets NACHT domain of NLRP3 (Fig. 3C). To confirm our findings, we used SPR and BLI to investigate the affinity between COS and purified NACHT protein. The SPR assay showed that COS interacted with recombinant NACHT proteins with a high affinity ($K_D = 7.615 \times 10^{-5}$ mol/L) (Fig. 3D). The BLI assay showed a similar affinity with a $K_D$ of $6.34 \times 10^{-5}$ mol/L (Fig. 3E). These data confirm the direct interaction between COS and NLRP3 NACHT domain.

NACHT is a critical domain for NLRP3 oligomerization through its ATPase activity, which is a vital step in the assembly of NLRP3 inflammasome[28]. We then detected the effect of COS on oligomerization of NLRP3 using semi-denaturing detergent agarose gel electrophoresis. The data showed that COS reduced NLRP3 oligomerization in BMDMs (Fig. 3F and Supporting Information Fig. S10). The ATPase activity of endogenous NLRP3 was then examined with or without COS treatment, which showed that COS dose-dependently suppressed NLRP3 ATPase activity (Fig. 3G), indicating that COS blocked NLRP3 oligomerization through an ATPase-dependent mechanism. These data indicated that COS directly interacts with NACHT domain, affecting its ATPase activity and subsequent NLRP3 oligomerization.

### 3.4. *COS covalently targets the cysteine 598 on NLRP3 NACHT domain*

Next, we investigated how COS binds to NACHT domain. Previous studies have shown the reactivity of $\alpha,\beta$-unsaturated carbonyl with thiols in targeted proteins *via* a Michael addition reaction, which often affords a covalent and irreversible binding between small molecules and proteins[29]. We can see that there is an $\alpha,\beta$-unsaturated carbonyl group in the COS structure. Then, we explored whether COS has an irreversible effect on NLRP3 inhibition. We treated COS with LPS-primed BMDMs for 15 min and then washed the cells thrice to remove the free small molecule. We found that COS keeps the inhibitory activity against IL-1$\beta$ and p20 production after washing, indicating that COS inhibits NLRP3 in an irreversible manner (Fig. 4A and B, and Supporting Information Fig. S11A). We then confirmed the contribution of $\alpha,\beta$-unsaturated carbonyl to the anti-NLRP3 activity of COS. We reduced the ethylene bond in $\alpha$, $\beta$-unsaturated carbonyl to give r-COS (Fig. 4C). As expected, r-COS failed to inhibit p20 cleavage and IL-1$\beta$ secretion in BMDMs (Fig. 4D, E, and Fig. S11B).

To decipher the COS-binding site in NLRP3, we expressed Flag-tagged NLRP3 in HEK-293T cells treated with COS, pulled NLRP3 protein, and performed HPLC-tandem mass spectrometry to detect the COS-modified peptide in NLRP3 and determine the precise amino acid to which COS covalently bound. According to the mass spectrometry analysis, we found that the peptide sequence of "KLSCK" had a modified mass with addition of 233.154, which is equal to the molecular mass of COS (Fig. 4F). BLAST analysis showed that the "KLSCK" sequence is located in NACHT domain of both human and mouse NLRP3. COS covalently binds to cysteine 598 in human NLRP3 or cysteine 596 in mouse NLRP3. We constructed a human NACHT plasmid with a C598 mutation to alanine (C598A). Pull-down assay using bio-COS showed that C598A mutation significantly reduced the interaction between COS and NACHT in HEK-293T cells (Fig. 4G). These results indicate that COS covalently binds to C598 in NACHT domain. We also examined the ATPase activity of NLRP3 C598A mutant to see the functional role of C598. As shown in Supporting Information Fig. S12A, C598A NACHT mutant shows much lower ATPase activity than the wild-type protein, indicating that C598 might be a critical residue for NLRP3 inflammasome activation. No additive protective effects were observed with COS treatment in C598A mutant (Fig. S12A). We further tested whether C598A mutant affects NLRP3 oligomerization in HEK-293T. The result shows that C598A mutant decreased NLRP3 oligomerization and COS cannot further enhance this trend (Fig. S12B).

Based on these results, we constructed a proposed model for the reaction between the $\alpha,\beta$-unsaturated carbonyl of COS and C598 residue of NLRP3 (Fig. 4H). Since we failed to obtain a crystal structure of COS−NLRP3 or COS−NACHT complex, we could only attempt to understand the COS−NLRP3 interaction at the molecular level by simulating a molecular model using docking software. The results show that an $\alpha$-helix containing C598 in NACHT plays a vital role in NLRP3 oligomerization, whereas covalent binding of COS−C598 may hinder NLRP3 oligomerization or dimerization and alter the function of NLRP3 ATPase activity (Fig. 4I and J).

### 3.5. *α-Methylene-γ-butyrolactone motif is an important group of inhibiting NLRP3 activation*

The importance of $\alpha,\beta$-unsaturated carbonyl group in $\alpha$-methylene-$\gamma$-butyrolactone motif of COS prompted us to investigate

analysis of NLRP3 NACHT domain oligomer. Two NACHT domains interacted at the $\alpha$-helix containing C598 (cartoon, PDB ID: 7ALV). (J) Molecular docking analysis of COS covalently bound to NLRP3. COS (sticks model) in the binding site C598 of NACHT domain (sticks and cartoon, PDB ID: 7ALV). Green color represents van der Waals' interactions. Data are presented as the mean ± SEM, $n = 3$; ***$P < 0.001$; ns, not significant.

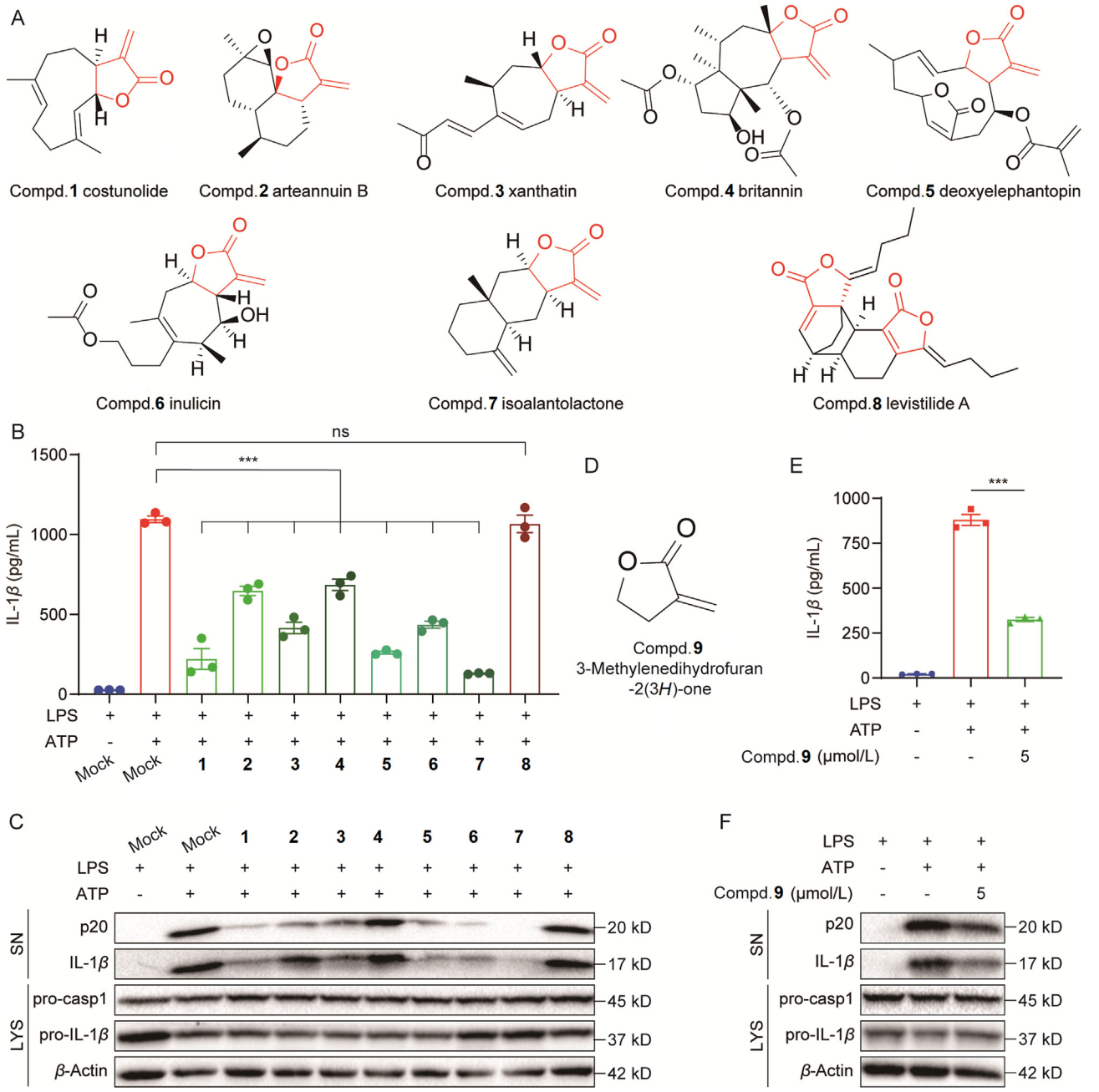


**Figure 5** Important role of α-methylene-γ-butyrolactone motif for the inhibition of NLRP3 activation. (A) Structures of the natural compounds screened from our in-house library, all of which have the α-methylene-γ-butyrolactone motif. (B, C) LPS-primed BMDMs were treated with various compounds for 30 min and stimulated with ATP for 30 min. ELISA of IL-1β in SN (B) or Western blotting analysis of cleaved IL-1β and p20 in SN (C). (D) Structure of 3-methylenedihydrofuran-2(3*H* )-one. (E, F) LPS-primed BMDMs were treated with 3-methylenedihydrofuran-2(3*H* )-one for 30 min then stimulated with ATP for 30 min. ELISA of IL-1β in SN (E) or Western blotting analysis of cleaved IL-1β and p20 in SN (F). Data are presented as the mean ± SEM, $n = 3$; ***$P < 0.001$; ns, not significant.

other natural compounds containing this motif. We collected several eligible natural compounds that contain the α-methylene-γ-butyrolactone motif in our in-house compounds bank, including arteannuin B, xanthatin, britannin, deoxyelephantopin, inulixin, isoalantolactone (Fig. 5A). We also selected a compound levistilide A, which contains a conformation-limited α-methylene in the α-methylene-γ-butyrolactone motif (Compd. **8**, Fig. 5A). We then examined the inhibitory effects of these compounds on inflammasome activation at 5 μmol/L in BMDMs and found that these compounds significantly inhibited p20 and IL-1β production, except levistilide A (Fig. 5B and C, and Supporting Information Fig. S13A). To confirm the role of this motif, we used a single compound α-methylene-γ-butyrolactone, 3-methylenedihydrofuran-2(3*H* )-one (Fig. 5D), and showed that this structure also significantly inhibited NLRP3 activation at 5 μmol/L in BMDMs, as evidenced by the reduced p20 and IL-1β levels (Figs. 5E, F, and S13B). Taken together, we present α-methylene-γ-butyrolactone as a functional motif for suppressing

NLRP3 activation and demonstrating the anti-NLRP3 activity of natural compounds including COS.

### 3.6. *COS inhibits NLRP3 activation in vivo and exerts preventive effects in mouse models of gouty arthritis and peritonitis*

NLRP3 inflammasome activation has been reported to drive the pathogenesis and development of gouty arthritis induced by MSU[13]. We created a mouse model of acute gout arthritis to assess the therapeutic efficacy of COS *in vivo*. As expected, MSU injection caused joint swelling over time in the footpad tissue of wild-type (WT) mice, whereas administration of COS significantly reduced the joint swelling in MSU-challenged mice (Fig. 6A and B). COS treatment also decreased the level of IL-1$\beta$ and p20 in the tissue culture supernatants, which was regarded as a signal of NLRP3 inflammasome in the diseased organ (Fig. 6C and D). H&E staining of the joint tissue showed that COS treatment suppressed histopathological changes and neutrophil influx in the footpad of MSU-challenged mice (Fig. 6E). Similar

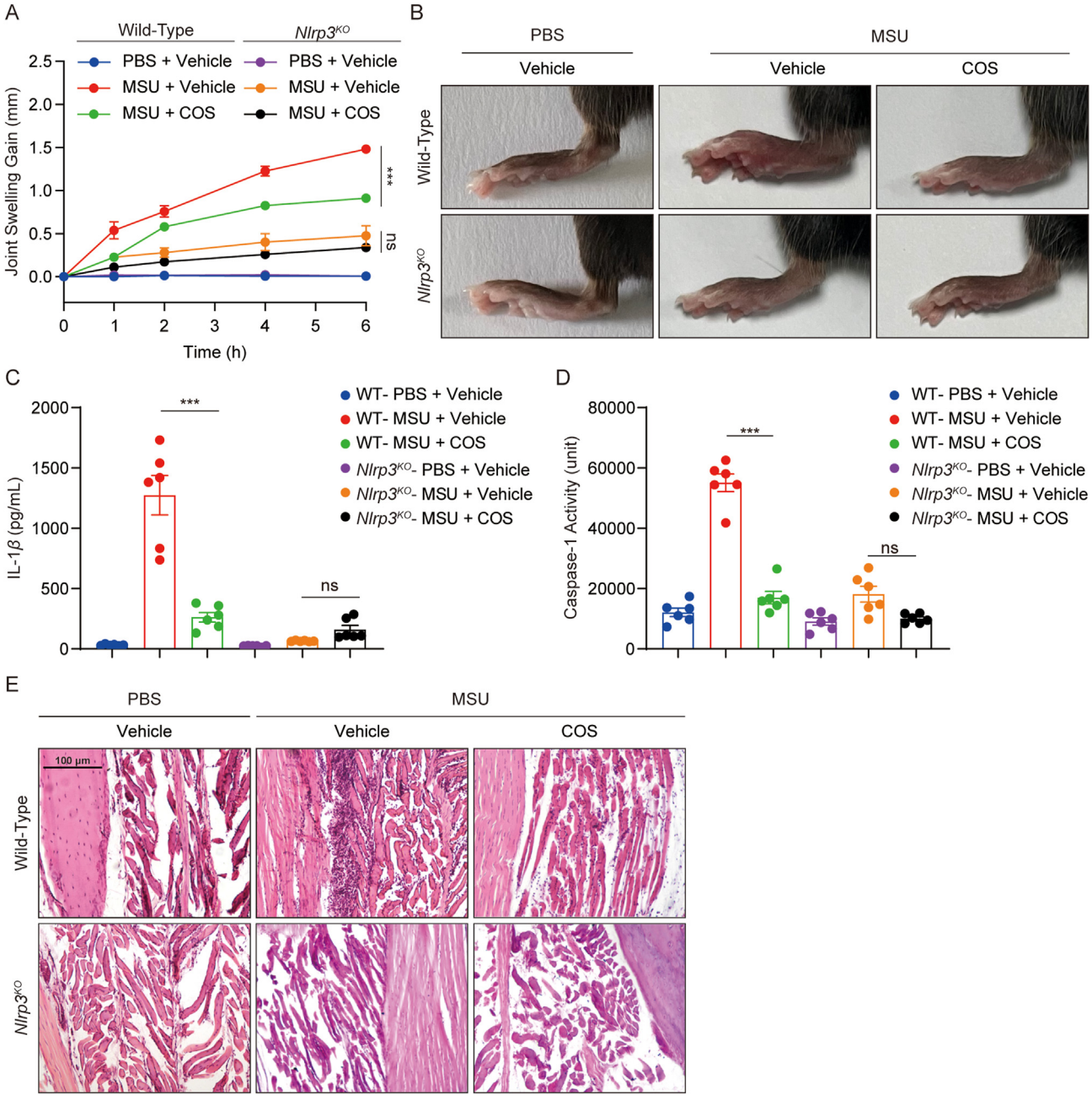


**Figure 6** COS exhibits preventive effects in mouse models of gouty arthritis. (A–E) 8–10-week-old male WT or *Nlrp3*$^{KO}$ mice were intra-footpad injected with MSU for 6 h. COS (40 mg/kg) or vehicle was administered before injection three times at 1 h intervals. (A) Time course of changes of joint swelling. (B) Representative photographs to show the swelling of joints. (C) ELISA of IL-1$\beta$ in the SN of the joint culture. (D) Activity of caspase-1 in the SN of the joint culture. (E) H&E-stained histological footpad tissues sections. Original magnification 100×. Data are presented as the mean ± SEM, $n = 6$ per group; ***$P < 0.001$; ns, not significant.

protection against MSU-induced gouty arthritis was observed in *Nlrp3*$^{KO}$ mice (Fig. 6A−E). Importantly, no additive protective effects were observed when MSU-challenged *Nlrp3*$^{KO}$ mice were treated with COS (Fig. 6A−E). Similarly, we found that COS treatment reduced neutrophils migration in WT mice model of Alum-induced peritonitis (Supporting Information Fig. S14A and S14B), and decreased the level of IL-1$\beta$ and p20 in the peritoneal lavage cells harvested from the peritonitis model (Fig. S14C), but the therapeutic efficacy of COS treatment was not observed in *Nlrp3*$^{KO}$ mice (Fig. S14A−S14C). These data indicate that NLRP3 mediates the anti-arthritis and anti-peritonitis effects of COS.

### 3.7. *COS alleviates DSS-induced ulcerative colitis in mice*

Studies have reported that NLRP3 inflammasome plays an important role in DSS-induced ulcerative colitis[30]. Therefore, we examined the pharmacological effects of COS in a mouse model of DSS-induced acute colitis. DSS challenge decreased body weight and increased DAI in mice, while COS therapy reduced body weight loss and DAI in DSS-challenged mice (Fig. 7A and B). Furthermore, COS prevented colon shortening, which is characteristic of colitis severity (Fig. 7C and Supporting Information Fig. S15A). DSS-induced IL-1$\beta$ production and p20 expression were also inhibited by COS treatment in WT mice, suggesting that COS prevents NLRP3 inflammasome activation *in vivo* (Figs. 7D, E, and S15B). H&E staining of colonic histopathology showed that COS therapy decreased crypt disappearance and inflammatory cell influx (Figs 7F and S15C). We also examined the protective effect of NLRP3 deficiency on colitis in mice. Similar effects against DSS-induced colitis were observed in *Nlrp3*$^{KO}$ mice (Figs. 7A−F and S15A−S15C). In addition, COS treatment failed to reduce IL-1$\beta$ production and p20 expression in colon tissues, and no additive pharmacological effects were observed when DSS-challenged *Nlrp3*$^{KO}$ mice were treated with COS (Figs. 7A−F and S15A−S15C). These results indicate that COS alleviates DSS-induced ulcerative colitis by inhibiting NLRP3.

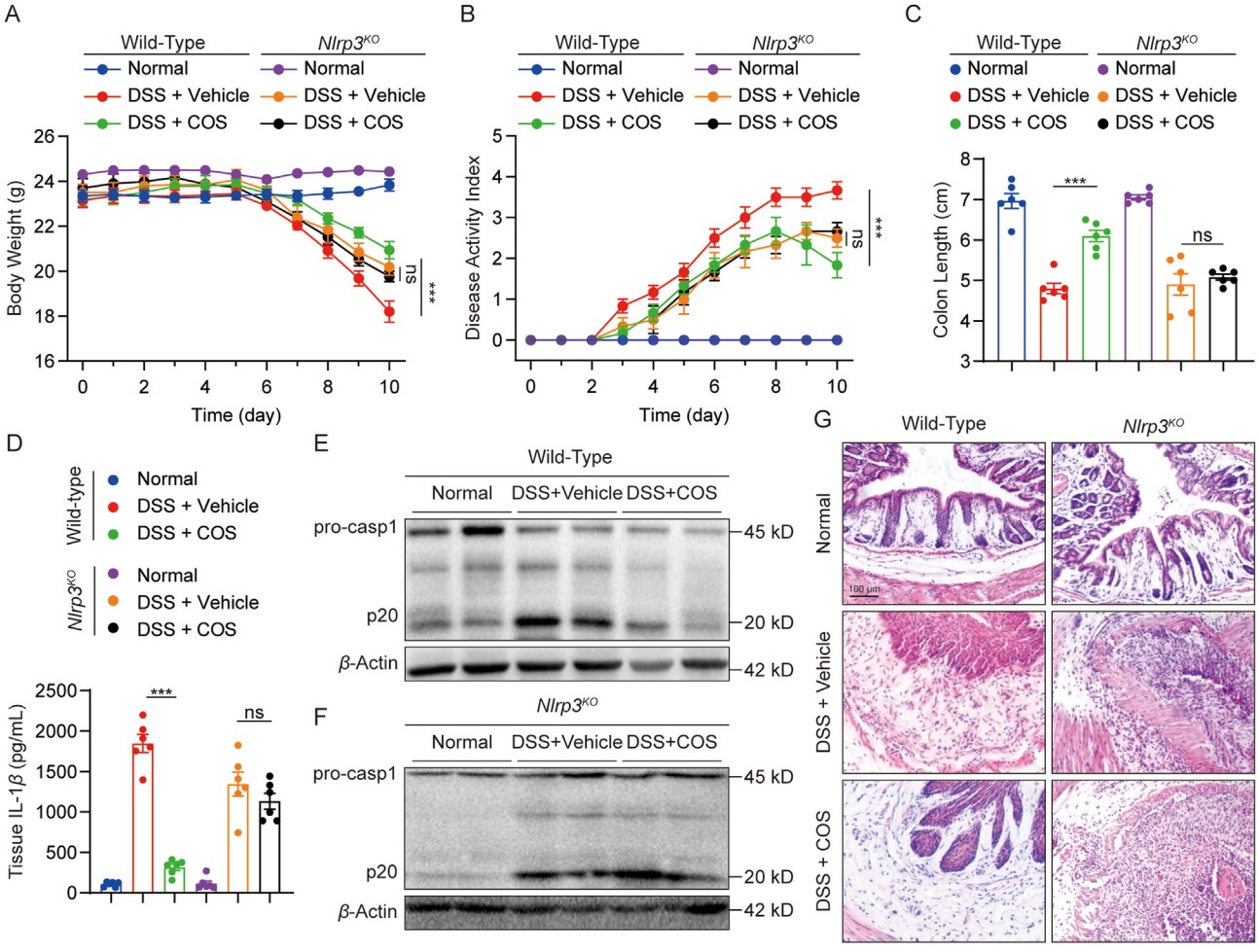


**Figure 7** COS inhibits NLRP3 activation *in vivo* and alleviates DSS-induced ulcerative colitis in mice. (A−F) 10-week-old male WT or *Nlrp3*$^{KO}$ mice were treated with 2.5% DSS dissolved in drinking water for six days and then provided normal drinking water for four days. COS (40 mg/kg) or vehicle was administered daily. (A) Bodyweight loss, (B) disease activity index (DAI), and (C) colon lengths were measured. (D) Tissue homogenates from colon IL-1$\beta$ levels were assessed using ELISA. (E) Western blot analysis of p20 and pro-caspase-1, and $\beta$-actin of tissue homogenates from the colon of WT or *Nlrp3*$^{KO}$ mice. (F) Sections of paraffin-embedded colon tissues were stained with H&E. Original magnification 100×. Data are presented as the mean ± SEM, $n = 6$ per group; ***$P < 0.001$; ns, not significant.

## 4. Discussion

In this study, we discovered that COS is a potent and selective inhibitor that covalently and directly binds to NLRP3. COS has remarkable anti-inflammasome activity in *vitro* and in *vivo*, suggesting that it might be exploited as a lead compound for the development of novel NLRP3-driven disease therapeutics. According to our results, COS directly binds to the NLRP3 NACHT domain with high affinity and covalently binds to C598, thereby reducing the ATPase activity of NLRP3. We also found that the α-methylene-γ-butyrolactone motif is crucial for natural products targeting cysteines in NLRP3, as it results in a strong irreversible anti-inflammasome action. Hence, this motif can be used to design novel NLRP3 inhibitors. Meanwhile, the complete NLRP3 structure is unavailable in the PDB. We aim to determine the precise mechanism of NLRP3 activation and to create a co-crystal structure.

Terpenoids are one of the major types of natural products inherent in traditional Chinese herbs that exhibit a wide range of anti-inflammatory effects[31,32]. COS, a well-known sesquiterpene lactone, exhibits anti-inflammatory activity[33]. COS has been reported to have anti-inflammatory effects owing to its negative effect on NF-κB and mitogen-activated protein kinase (MAPK) signaling, and its ability to abrogate oxidative stress by modulating heme oxygenase-1 signaling[34]. Kang et al.[25] found that COS suppressed NF-κB activation in LPS-stimulated RAW264.7 cells by targeting IκBα phosphorylation[26]. According to Butturini et al.[35], COS reduces IL-1β expression *via* MAPK phosphorylation and activator protein transcription. Likewise, COS inhibits the phosphorylation and DNA-binding activity of the signal transducer and activator of transcription-3 by downregulating of the Janus-activated kinase-1 and -2 levels in human THP-1 cells. Recently, Liu et al.[36] reported that COS significantly inhibits neuroinflammation in BV2 microglial cells by targeting the cyclin-dependent kinase 2. However, we did not observe an evident decline in TNF-α levels in LPS/ATP-challenged BMDMs' supernatant and LPS-challenged mice's serum, suggesting that the concentrations and action time of COS required to inhibit NLRP3-mediated IL-1β production were substantially lower than the limits of TNF-α production. Higher concentrations and prolonged administration periods may produce off-target effects during treatment, resulting in other uncontrollable biological activities. Therefore, it is important to improve the bioavailability and NLRP3-targeting ability of COS to promote its clinical application.

The NACHT domain's ATPase activity is vital for NLRP3 self-association and function[37]. Several drugs targeting NLRP3 have been identified as selective inhibitors of inflammasome activation. Coll et al.[38] developed the first synthetic small-molecule inhibitor of NLRP3, MCC950. MCC950 has been proven to be effective in blocking NLRP3 activation at nanomolar concentrations by inhibiting ATP hydrolysis activity of NACHT[39]. Jiang et al.[40] reported that CY-09, a potent inhibitor of the NLRP3, suppresses the ATPase activity of NACHT. Tranilast inhibits inflammasome activation by preventing NLRP3 self-oligomerization by targeting NACHT[41]. Some natural products derived from traditional Chinese herbs, such as parthenolide[42] and oridonin[22], also have substantial and specific inhibitory effects on NLRP3 inflammasome activation. Interestingly, NACHT domain seems to be the most likely target of molecular inhibitors, according to the finding that numerous inhibitors target NACHT domain or affect the ATPase activity. We also found that COS binds to NACHT domain, indicating that NACHT is the most significant pharmacological target for NLRP3. ATPase activity is necessary for ASC association and NLRP3 oligomerization; thus, the inhibition of NLRP3 ATP function might aid in the development of NLRP3 inhibitors. COS irreversible suppressed the ATPase activity of NLRP3, suggesting that it exhibits better inhibitory effects than the presently available inhibitors.

Here, we identified a molecule that could suppress NLRP3 activation by covalently binding to C598 for the first time. Although binding to cysteine 279 has been reported as a strategy to inhibit NLRP3 activity[22], the targeting potential of other cysteines in NACHT remains unclear. We found that C598 might be a critical residue of NLRP3 inflammasome activation since the ATPase activity and the self-oligomerization of C598A NLRP3 mutant was much lower than that of wild-type NLRP3. In our simulation models, C598 was positioned near the polymerization site of the NLRP3 homodimer, and small molecule modifications to C598 might alter both the conformation and function of NLRP3. We observed that C598 is located on the rear end of NACHT, close to LRR, which might explain why COS could block the interaction between NEK7 and NLRP3, indicating that it could be a target for the development of inhibitors. However, the specific function of NACHT needs to be clarified *via* future structural biology studies.

We found that COS might be a potential lead compound for the design of NLRP3-covalent inhibitors and that targeting the α-methylene-γ-butyrolactone motif could be a promising direction for future research on the design of novel NLRP3 inhibitors. In recent years, the US Food and Drug Administration has approved many covalent drugs, including telaprevir (2010) for hepatitis C virus infection targeting HCV protease[43], afatinib (2013) for non-small-cell lung cancer by inhibiting the ErbB family[44], ibrutinib (2013) for chronic lymphocytic leukemia as Bruton's tyrosine kinase inhibitor[45], and osimertinib (2015) for non-small cell lung cancer by targeting the epidermal growth factor receptor[46]. The advantages of covalent drugs include enhanced potency and a prolonged duration of action[47]. However, the indiscriminate reactivity and off-target effects have caused many researchers to shy away from developing covalent drugs. At higher concentrations, the inhibitory effects of COS on NF-κB or MAPK signaling may be activated during the treatment of inflammatory disease process. Off-target effects under a higher dose can be avoided *via* improvements in pharmacodynamics, pharmacokinetics, and bioavailability, which will be explored further in future studies. The multiple anti-inflammatory activities and possible multi-targets of COS, especially the synergistic inhibition of inflammation-related signals, may strengthen its development and clinical application.

Structure-based drug modification is another method to improve COS and discover excellent derivatives of COS. Our data show that the α-methylene-γ-butyrolactone motif is the certain active group in binding to NACHT C598 and inhibiting NLRP3 activation, which supports it as a promising lead structural core for designing and discovering new NLRP3 inhibitors. The α-methylene-γ-butyrolactone motif must be of weak selectivity since it is just a very small and simple lead skeleton. Chemical modification from α-methylene-γ-butyrolactone motif will enhance the NLRP3-inhibiting selectivity. We believe that, further drug design and chemical modification based on COS will obtain specific small-molecule inhibitors with a much higher affinity with NLRP3.

## 5. Conclusions

In summary, our study, for the first time, reported that COS covalently binds to C598 of NLRP3 NACHT domain, altering the ATPase activity and assembly of NLRP3 inflammasome. COS showed great anti-inflammasome efficacy in mouse models of gouty arthritis and ulcerative colitis by inhibiting NLRP3 inflammasome activation. We also discovered that the $\alpha$-methylene-$\gamma$-butyrolactone motif in sesquiterpene lactone is an active group that inhibits NLRP3 activation, which may help to design and develop novel NLRP3 inhibitors.

## Acknowledgments

This study was supported by the National Natural Science Foundation of China (81930108 to Guang Liang, 82000793 to Wu Luo, and 82170373 to Yi Wang), Natural Science Foundation of Zhejiang Province (LY22H070004 to Wu Luo, China), Zhejiang Provincial Key Scientific Project (2021C03041 to Guang Liang, China), and Wenzhou Scientific Project in China (Y20210213 to Wu Luo).

## Author contributions

Guang Liang and Wu Luo contributed to the literature search and study design. Guang Liang, Wu Luo and Haowen Xu participated in the drafting of the article. Haowen Xu, Jiahao Chen, Pan Chen, Weifeng Li, Jingjing Shao, Shanshan Hong, and Lingfeng Chen carried out the experiments. Guang Liang and Yi Wang revised the manuscript. Wu Luo and Haowen Xu contributed to data collection and analysis.

## Conflicts of interest

The authors declare no conflicts of interest.

## Appendix A. Supporting information

Supporting data to this article can be found online at https://doi.org/10.1016/j.apsb.2022.09.014.

## References

1. Davis BK, Wen H, Ting JP. The inflammasome NLRs in immunity, inflammation, and associated diseases. *Annu Rev Immunol* 2011;**29**:707−35.
2. Liu X, Zhang Z, Ruan J, Pan Y, Magupalli VG, Wu H, et al. Inflammasome-activated gasdermin D causes pyroptosis by forming membrane pores. *Nature* 2016;**535**:153−8.
3. Chen G, Shaw MH, Kim YG, Nuñez G. NOD-like receptors: role in innate immunity and inflammatory disease. *Annu Rev Pathol* 2009;**4**:365−98.
4. Burdette BE, Esparza AN, Zhu H, Wang S. Gasdermin D in pyroptosis. *Acta Pharm Sin B* 2021;**11**:2768−82.
5. Kelley N, Jeltema D, Duan Y, He Y. The NLRP3 inflammasome: an overview of mechanisms of activation and regulation. *Int J Mol Sci* 2019;**20**:3328.
6. Pétrilli V, Papin S, Dostert C, Mayor A, Martinon F, Tschopp J. Activation of the NALP3 inflammasome is triggered by low intracellular potassium concentration. *Cell Death Differ* 2007;**14**:1583−9.
7. Tang T, Lang X, Xu C, Wang X, Gong T, Yang Y, et al. CLICs-dependent chloride efflux is an essential and proximal upstream event for NLRP3 inflammasome activation. *Nat Commun* 2017;**8**:202.
8. Zhou R, Yazdi AS, Menu P, Tschopp J. A role for mitochondria in NLRP3 inflammasome activation. *Nature* 2011;**469**:221−5.
9. Jin C, Flavell RA. Molecular mechanism of NLRP3 inflammasome activation. *J Clin Immunol* 2010;**30**:628−31.
10. Jiang H, Gong T, Zhou R. The strategies of targeting the NLRP3 inflammasome to treat inflammatory diseases. *Adv Immunol* 2020;**145**:55−93.
11. Shi H, Wang Y, Li X, Zhan X, Tang M, Fina M, et al. NLRP3 activation and mitosis are mutually exclusive events coordinated by NEK7, a new inflammasome component. *Nat Immunol* 2016;**17**:250−8.
12. Zhen Y, Zhang H. NLRP3 inflammasome and inflammatory bowel disease. *Front Immunol* 2019;**10**:276.
13. Szekanecz Z, Szamosi S, Kovács GE, Kocsis E, Benkő S. The NLRP3 inflammasome−interleukin 1 pathway as a therapeutic target in gout. *Arch Biochem Biophys* 2019;**670**:82−93.
14. Grebe A, Hoss F, Latz E. NLRP3 inflammasome and the IL-1 pathway in atherosclerosis. *Circ Res* 2018;**122**:1722−40.
15. Wei J, Zhao Y, Liang H, Du W, Wang L. Preliminary evidence for the presence of multiple forms of cell death in diabetes cardiomyopathy. *Acta Pharm Sin B* 2022;**12**:1−17.
16. Masters SL, Dunne A, Subramanian SL, Hull RL, Tannahill GM, Sharp FA, et al. Activation of the NLRP3 inflammasome by islet amyloid polypeptide provides a mechanism for enhanced IL-1$\beta$ in type 2 diabetes. *Nat Immunol* 2010;**11**:897−904.
17. Shao BZ, Xu ZQ, Han BZ, Su DF, Liu C. NLRP3 inflammasome and its inhibitors: a review. *Front Pharmacol* 2015;**6**:262.
18. Atanasov AG, Zotchev SB, Dirsch VM, Supuran CT. Natural products in drug discovery: advances and opportunities. *Nat Rev Drug Discov* 2021;**20**:200−16.
19. Pandey MM, Rastogi S, Rawat AK. *Saussurea costus*: botanical, chemical and pharmacological review of an ayurvedic medicinal plant. *J Ethnopharmacol* 2007;**110**:379−90.
20. Kim DY, Choi BY. Costunolide—a bioactive sesquiterpene lactone with diverse therapeutic potential. *Int J Mol Sci* 2019;**20**:2926.
21. Alotaibi AA, Bepari A, Assiri RA, Niazi SK, Nayaka S, Rudrappa M, et al. Saussurea lappa exhibits anti-oncogenic effect in hepatocellular carcinoma, HepG2 cancer cell line by Bcl-2 mediated apoptotic pathway and mitochondrial cytochrome *c* release. *Curr Issues Mol Biol* 2021;**43**:1114−32.
22. He H, Jiang H, Chen Y, Ye J, Wang A, Wang C, et al. Oridonin is a covalent NLRP3 inhibitor with strong anti-inflammasome activity. *Nat Commun* 2018;**9**:2550.
23. Lefebvre C, Rubez G, Khartabil H, Boisson JC, Contreras-García J, Hénon E. Accurately extracting the signature of intermolecular interactions present in the NCI plot of the reduced density gradient *versus* electron density. *Phys Chem Chem Phys* 2017;**19**:17928−36.
24. Lu T, Chen F. Multiwfn: a multifunctional wavefunction analyzer. *J Comput Chem* 2012;**33**:580−92.
25. Kang JS, Yoon YD, Lee KH, Park SK, Kim HM. Costunolide inhibits interleukin-1 beta expression by down-regulation of AP-1 and MAPK activity in LPS-stimulated RAW 264.7 cells. *Biochem Biophys Res Commun* 2004;**313**:171−7.
26. Koo TH, Lee JH, Park YJ, Hong YS, Kim HS, Kim KW, et al. A sesquiterpene lactone, costunolide, from Magnolia grandiflora inhibits NF-kappa B by targeting I kappa B phosphorylation. *Planta Med* 2001;**67**:103−7.
27. Duncan JA, Bergstralh DT, Wang Y, Willingham SB, Ye Z, Zimmermann AG, et al. Cryopyrin/NALP3 binds ATP/dATP, is an ATPase, and requires ATP binding to mediate inflammatory signaling. *Proc Natl Acad Sci U S A* 2007;**104**:8041−6.
28. Mariathasan S, Weiss DS, Newton K, McBride J, O'Rourke K, Roose-Girma M, et al. Cryopyrin activates the inflammasome in response to toxins and ATP. *Nature* 2006;**440**:228−32.
29. Jackson PA, Widen JC, Harki DA, Brummond KM. Covalent modifiers: a chemical perspective on the reactivity of $\alpha,\beta$-unsaturated carbonyls with thiols *via* Hetero-Michael addition reactions. *J Med Chem* 2017;**60**:839−85.

30. Lv Q, Xing Y, Liu J, Dong D, Liu Y, Qiao H, et al. Lonicerin targets EZH2 to alleviate ulcerative colitis by autophagy-mediated NLRP3 inflammasome inactivation. *Acta Pharm Sin B* 2021;**11**: 2880−99.
31. Hortelano S, González-Cofrade L, Cuadrado I, de Las Heras B. Current status of terpenoids as inflammasome inhibitors. *Biochem Pharmacol* 2020;**172**:113739.
32. Yan T, Yan N, Wang P, Xia Y, Hao H, Wang G, et al. Herbal drug discovery for the treatment of nonalcoholic fatty liver disease. *Acta Pharm Sin B* 2020;**10**:3−18.
33. Ju Z, Li M, Xu J, Howell DC, Li Z, Chen FE. Recent development on COX-2 inhibitors as promising anti-inflammatory agents: the past 10 years. *Acta Pharm Sin B* 2022;**12**:2790−807.
34. Pae HO, Jeong GS, Kim HS, Woo WH, Rhew HY, Kim HS, et al. Costunolide inhibits production of tumor necrosis factor-alpha and interleukin-6 by inducing heme oxygenase-1 in RAW264.7 macrophages. *Inflamm Res* 2007;**56**:520−6.
35. Butturini E, Cavalieri E, de Prati AC, Darra E, Rigo A, Shoji K, et al. Two naturally occurring terpenes, dehydrocostuslactone and costunolide, decrease intracellular GSH content and inhibit STAT3 activation. *PLoS One* 2011;**6**:e20174.
36. Liu YC, Feng N, Li WW, Tu PF, Chen JP, Han JY, et al. Costunolide plays an anti-neuroinflammation role in lipopolysaccharide-induced BV2 microglial activation by targeting cyclin-dependent kinase 2. *Molecules* 2020;**25**:2840.
37. Swanson KV, Deng M, Ting JP. The NLRP3 inflammasome: molecular activation and regulation to therapeutics. *Nat Rev Immunol* 2019; **19**:477−89.
38. Coll RC, Robertson AA, Chae JJ, Higgins SC, Muñoz-Planillo R, Inserra MC, et al. A small-molecule inhibitor of the NLRP3 inflammasome for the treatment of inflammatory diseases. *Nat Med* 2015;**21**:248−55.
39. Coll RC, Hill JR, Day CJ, Zamoshnikova A, Boucher D, Massey NL, et al. MCC950 directly targets the NLRP3 ATP-hydrolysis motif for inflammasome inhibition. *Nat Chem Biol* 2019;**15**:556−9.
40. Jiang H, He H, Chen Y, Huang W, Cheng J, Ye J, et al. Identification of a selective and direct NLRP3 inhibitor to treat inflammatory disorders. *J Exp Med* 2017;**214**:3219−38.
41. Huang Y, Jiang H, Chen Y, Wang X, Yang Y, Tao J, et al. Tranilast directly targets NLRP3 to treat inflammasome-driven diseases. *EMBO Mol Med* 2018;**10**:e8689.
42. Juliana C, Fernandes-Alnemri T, Wu J, Datta P, Solorzano L, Yu JW, et al. Anti-inflammatory compounds parthenolide and Bay 11-7082 are direct inhibitors of the inflammasome. *J Biol Chem* 2010;**285**:9792−802.
43. Kiang TK, Wilby KJ, Ensom MH. Telaprevir: clinical pharmacokinetics, pharmacodynamics, and drug−drug interactions. *Clin Pharmacokinet* 2013;**52**:487−510.
44. Harvey RD, Adams VR, Beardslee T, Medina P. Afatinib for the treatment of EGFR mutation-positive NSCLC: a review of clinical findings. *J Oncol Pharm Pract* 2020;**26**:1461−74.
45. Bond DA, Woyach JA. Targeting BTK in CLL: beyond ibrutinib. *Curr Hematol Malignant Rep* 2019;**14**:197−205.
46. Remon J, Steuer CE, Ramalingam SS, Felip E. Osimertinib and other third-generation EGFR TKI in EGFR-mutant NSCLC patients. *Ann Oncol* 2018;**29**:i20−7.
47. Singh J, Petter RC, Baillie TA, Whitty A. The resurgence of covalent drugs. *Nat Rev Drug Discov* 2011;**10**:307−17.